Production and Properties of Solvent-Cast Poly(ε-caprolactone) Composites with Carbon Nanostructures

M. Dottori,[1] I. Armentano,[2] E. Fortunati,[2] J. M. Kenny[1,2]

[1]*Biostructures and Biosystems Institute I.N.B.B. at Material Science and Technology Center, University of Perugia, Terni, Italy*
[2]*Material Science and Technology Center, UdR INSTM, NIPLAB, University of Perugia, Terni, Italy*

Received 21 December 2009; accepted 1 July 2010
DOI 10.1002/app.33033
Published online 30 September 2010 in Wiley Online Library (wileyonlinelibrary.com).

ABSTRACT: Composites based on carbon nanostructures (CNS) and poly(ε-caprolactone) (PCL) were produced by solvent casting technique. Single-walled carbon nanotubes (SWCNTs) and carbon nanofibers (CNFs) were selected, to produce composite films with enhanced properties. The role of CNS type and percentage were investigated in terms of morphological, thermal, mechanical, and dielectrical properties. Composite morphological analysis reveals a good dispersion of CNS, at low and high content. Thermal properties underline the nucleation effect of CNS on PCL polymer matrix. Reinforcing effects in terms of increased tensile modulus were obtained with both nanofillers, but a higher reduction of the ductility was shown in PCL/CNF materials. A higher efficiency to form a conductive network, assessed by AC conductivity, was observed for SWCNTs at concentration lower than 1 wt. %

Key words: biopolymers; nanocomposites; mechanical properties; dielectric properties

INTRODUCTION

Nanostructured polymers and composites have become a great challenge for scientists to create novel systems with enhanced physical and chemical properties.[1,2] The fast development of electronic technology has brought about a demand for materials with enhanced physical and mechanical properties. In particular functional polymer composites based on a wide range fillers, have been extensively explored and applied to modify and improve the electrical conductivity.[3–5] In the last decade, an increasing attention has been given to polymer composites based on natural or synthetic biodegradable polymer matrices.[6–8] Among these matrices, poly(ε-caprolactone) (PCL), an aliphatic semicrystalline polyester, is been employed in a wide range of applications, such as biodegradable materials for packaging,[9] implants,[10] and microparticles for drug delivery.[11] Considerable research efforts have been focused recently on the enhancement of polymer mechanical and electrical properties by the introduction of carbon nanostructures (CNS) such as carbon nanotubes and nanofibers.[12–17]

CNS can be classified as a function of their different structure and nanoscale dimensions: zero-dimensional structures (fullerenes, diamond clusters), one-dimensional (carbon nanotubes, carbon nanofibers, diamond nanorods), two-dimensional (graphite sheets, diamond nanoplatelets), and three-dimensional structures (nanocrystalline diamond films, fullerite).[18] CNS are considered to be the ideal reinforcing agents for high-strength polymer composites, because of the excellent mechanical strength, high electrical conductivity, and high aspect ratio.[19–21] Among them, carbon nanotubes (CNTs) have grabbed the attention of researchers and technologists for the production of polymer matrix materials with enhanced properties as compared to conventional microcomposites.[22,23]Attention has been recently also given to carbon nanofibers (CNFs), which are nanostructures consisting of continuous graphene ribbons rolled in cylindrical or conical tubes, with diameter in the order of 100 nm and lengths ranging from less than a micron to millimeters, whereby, they can mismatch with the interface layer in hybrid systems.[24] However, simple nanofiller addition does not guarantee the achievement of enhanced properties; novel ultra-high strength polymer composites demand a uniform dispersion of the nanofillers in the polymer matrix and a strong interaction between CNS and polymer is needed.[25–27]

A huge number of scientific publications have been focused on the electrical properties of carbon nanotube polymer composites and on their electrical percolation threshold.[28,29] Regarding PCL, the

Correspondence to: I. Armentano (Ilaria.armentano@unipg.it).

increase of its conductivity with 3% wt of single-walled carbon nanotubes (SWCNTs) and sonication was reported.[29] Moreover, the nucleation effects and the induction of a hierarchical morphology in a PCL matrix composites with aligned SWCNTs associated to a significant mechanical reinforcement of the polymer has been reported.[30]

Few articles have been focused on composites based on PCL and functionalized CNFs,[31,32] while we recently reported the comparison of PCL/CNF composites prepared with different processing conditions (electrospinning versus solvent casting).[20]

In particular, the solvent casting process is a conventional, flexible, low-cost, and short-term process widely used for the fabrication of polymeric composite films based on biodegradable polymers (PLGA, PLLA, PCL, etc.) and nanostructures. In composite development by solvent casting process, the effects of the solvents used for the realization of films need to be elucidated. Specific properties of solvent (i.e., electron-pair donicity, solvochromic parameter, hydrogen bond donation parameter, and dielectric constant) can support an effective dispersion of nanostructures in the solvent and consequently in the polymer matrix.[33]

In this article, we report the development of PCL/CNS composites and their morphological, mechanical, thermal, and electrical properties to elucidate the effects of different CNS on PCL properties and to take advantage of the unique combination of electrical and mechanical properties that CNS provide to PCL matrix composites.

EXPERIMENTAL

Materials

Poly(ε-caprolactone) (PCL, M_n = 80,000) was supplied by Sigma-Aldrich (Germany). Two CNS were considered in the present work: SWCNTs and CNFs. SWCNTs black powders were obtained from Thomas Swan & Co. Ltd (Elicarb^{TM}, Durham, UK). CNFs, HHT Grade, were purchased from Pyrograf® with an iron content less than 400 ppm. Thermal characterization of CNS was carried out by thermogravimetric analysis (TGA) on a Seiko Exstar 6000 quartz rod microbalance, in air flow (50 mL/min) from 30 to 1000°C with a 5°C/min heating rate.

The CNS morphology was investigated by means of field emission scanning electron microscopy (FESEM, Supra 25-Zeiss, Germany). CNS samples were prepared by dispersion in *N*,*N*-dimethylformamide (DMF) through ultrasonic mixing (Ultrasonic bath, EMMEGI mod.AC-5). CNS were sonically dispersed in DMF (0.1 mg/mL) for 4 h, few drops of CNS suspension were placed onto silicon substrate and they were vacuum dried for 2 h.

Preparation of PCL/CNS nanohybrid films

PCL and PCL/CNS nanohybrid films were produced by solvent casting technique. The same procedure was applied in both carbon nanotube and nanofiber-based composites. CNFs or SWCNTs, were dispersed in chloroform ($CHCl_3$, Carlo Erba Reagenti, Italy) by means of sonication treatment. The ultrasonic bath was used to reduce CNS bundles, to increase dispersion in the solvent, and to improve the interaction with the PCL matrix. The polymer (1 g) was finally added to CNS/$CHCl_3$ dispersion and the suspension was magnetically stirred to dissolve the polymer. The polymer/solvent ratio was chosen as 10% (w/v). The obtained dispersions were cast on Teflon sheet and 50 mm × 50 mm and 0.3-mm thick composite films, were produced, after solvent evaporation. Samples were air dried for 48 h and vacuum dried for 24 h at room temperature (RT).

Different CNS percentages were introduced in the PCL polymer matrix in consideration of the property modulation. PCL/CNF samples were prepared with the addition of 0.5, 1, 3, or 7% wt as respect to PCL initial weight and designed as PCL0.5f, PCL1f, PCL3f, PCL7f, respectively. PCL/SWCNT samples were prepared with the addition of 0.5, 0.75, or 1% wt respect to PCL weight and designed as PCL0.5t, PCL0.75t, PCL1t, respectively. Neat PCL film was also prepared by solvent casting for comparison.

The composites based on SWCNTs were realized with concentration until 1% wt, while in the case of CNFs higher concentration were used, as previously reported.[12–17,34,35]

Investigation of PCL/CNS morphology

PCL/CNS composite structure was investigated by field emission scanning electron microscopy (FESEM, Supra 25-Zeiss, Germany) to evaluate the CNS dispersion in the polymer. No metallization was required. FESEM images were performed on the surface and on the on cross section samples, after they were fractured in liquid nitrogen.

Investigation of PCL/CNS thermal properties

TGA and differential scanning calorimetry (DSC) were carried out, to assess the influence of CNS on thermal properties of the polymer. TGA was performed on 10-mg samples, with nitrogen flow of 250 mL/min, at 10°C/min heating rate, from 30 to 900°C. The residual mass and thermal degradation temperature (T_d) were calculated.

DSC measurements were performed at 10°C/min, from −25 to 100°C, two heating and one cooling scans were carried out. Melting enthalpy (ΔH_m) and temperature (T_m) were calculated from the heating scans, while crystallization enthalpy (ΔH_c) and temperature (T_c) were evaluated from the cooling scan.

T_m represents the maximum temperature of endothermic peak in the heating scan, while the T_c is the maximum temperature of the exothermic peak in the cooling scans; ΔH_m and ΔH_c were calculated as the integral under the melting and cooling peaks, respectively. The PCL crystallinity degree (χ) was calculated according to the following relation:

$$\chi(\%) = \frac{1}{(1 - m_f)} \frac{\Delta H}{\Delta H_0} \cdot 100 \quad (1)$$

where ΔH is the scan-related enthalpy, ΔH_0 is the reference enthalpy, defined as heat of a 100% PCL crystalline sample, 136 J/g[36] and m_f represents the theoretical weight fraction of CNS in the nanohybrid samples.

Mechanical properties

The mechanical behavior of neat PCL and hybrid PCL/CNS films was evaluated by failure tensile test and dynamo-mechanical analysis (DMA).

Failure tensile test was carried out with a digital Lloyd instrument LR 30K (UK), at a cross-head speed of 5 mm/min and samples with dimensions of 50 mm × 10 mm and 0.3-mm thickness. Tensile strength (σ_b), failure strain (ε_b), yield strength (σ_y) and yield strain (ε_y) were measured from the stress–strain curves. The Young modulus (E) was calculated between 0 and 0.05 strain.

Dynamo-mechanical analysis (DMA) was performed by a Rheometric Scientific-ARES N_2. Measurements were realized in the dynamic time sweep test, at a frequency of 1 Hz, at RT. The shear strain was selected at 0.3% in the elastic linear region. Samples with dimensions of 50 mm × 10 mm and 0.3-mm thickness were tested. Shear modulus (G′) of PCL and PCL composites was measured. Data are expressed as mean value ± mean standard deviation, calculated on a set of five samples.

Dielectric characterization

Dielectric measurements were performed by HP 4284A precision LCR meter (Hewlett–Packard, USA), in the 20 Hz ÷ 1 MHz frequency range, with a voltage amplitude of 0.5 V, at RT. Neat PCL and composite samples were placed between two copper-plated electrodes, the real part (Z_r), the imaginary part (Z_i), the module ($|Z|$) and the phase (θ) of the impedance were measured. The specific bulk conductivity σ_{ac} was calculated according to:

$$|\sigma_{ac}| = \frac{1}{|Z|} \cdot \frac{d}{A} \quad (2)$$

where A is the contact area, d is the sample thickness, and $|Z|$ is the complex impedance module as a function of frequency.

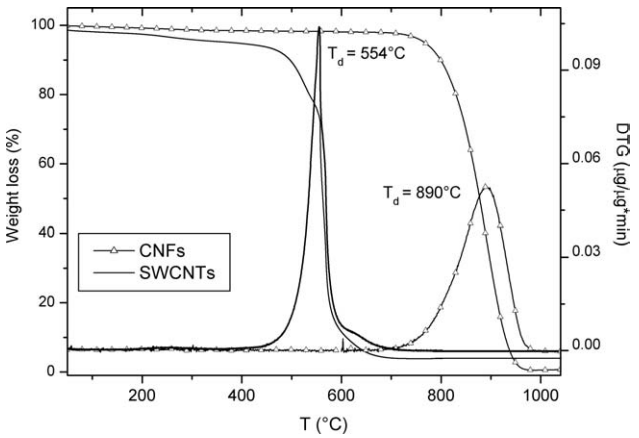

Figure 1 Thermogravimetric analysis (TGA) of CNFs and SWCNTs.

Statistical analysis

Data are expressed as mean ± standard deviation. Statistical analysis was performed by means of Student's *t*-test to determine significant differences in the thermal, mechanical, and electrical values between the neat polymer and composites. Significant level was set at $P < 0.05$.

RESULTS AND DISCUSSION

CNS characterization

The results of the CNS TGA, in air flow, are shown in Figure 1. The time derivative weight loss curve (DTG) shows that only one main weight loss step characterizes the CNS degradation. Residual mass of 0.6% wt for CNFs and 3.6% wt for SWCNTs at 1000°C were detected, and can be attributed to the residual metal catalysts. Absence of any weight loss in the low temperature region, that is, between 300 and 400°C suggests the absence of amorphous carbon in the samples.[37] The main thermal degradation temperature (T_d) in the SWCNTs is at 554°C. The weight loss at higher temperature in the SWCNT indicates that other structured carbon may also be present, as these tubes decompose at temperatures higher than those for SWCNTs.[38]

The CNF thermal stability is high, since a temperature purification treatment was applied to CNFs from Pyrograf. Thermal stability is a good measure of the overall quality in a given nanostructure sample. The high degradation temperature (890°C) is always associated with pure, less-defective samples. The low residual mass indicates an high purity level of the CNS.[39] FESEM image in Figure 2(a) reveals that CNFs are individually separated and characterized by a cylindrical structure, with diameters ranging from 100 to 200 nm, as reported in the Pyrograf datasheet. Figure 2(b) shows that SWCNTs are

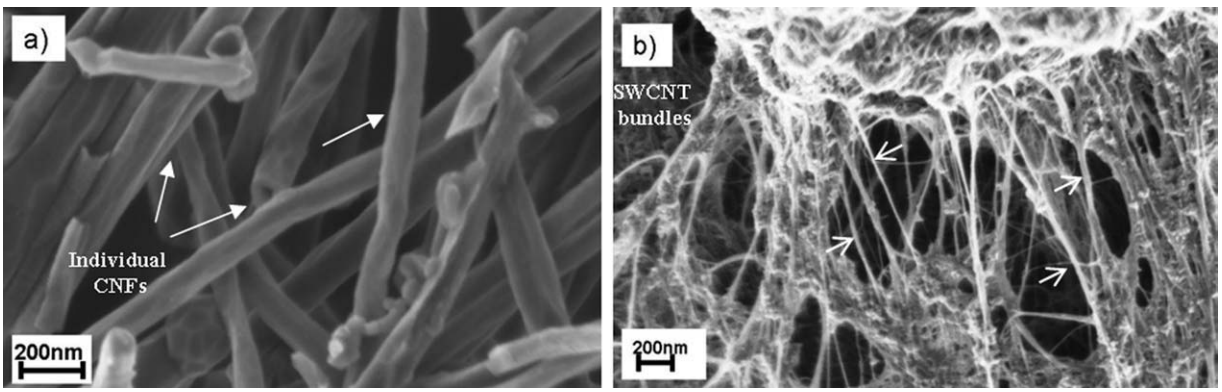

Figure 2 FESEM images of the CNFs (a) and SWCNTs bundles (b) at high magnification.

aggregated in ropes with about 10-nm diameter. CNS FESEM images show a large number of fiber-like particles, partially de-bundled.[40] Arrows in the images underline the presence of SWCNT bundles and individual CNFs.

PCL/CNS nanohybrid structure

Figure 3 shows FESEM images of PCL/CNS at low and high magnification. Low resolution image of PCL1t shows a large amount of SWCNT bundles immersed in the polymer matrix. A SWCNT random dispersion was revealed in the PCL1t composites [Fig. 3(a,b)].

A homogeneous CNF dispersion is revealed in the PCL1f and PCL3f samples [Fig. 3(c–f)].

CNFs are individually separated and the PCL polymeric matrix wraps around CNFs. The micrographs [Fig. 3(c,e)] show homogeneous CNF dispersion in the polymer and a partial CNF alignment that can affect composite properties. It should be noted that also at higher contents (PCL7f), CNFs are uniformly dispersed in the matrix, as previously shown.[20]

Thermal investigation

Figure 4 shows the cooling and the second melting scans of PCL, PCL1f, and PCL1t, to compare the effects of SWCNTs and CNFs on PCL thermal properties. DSC data of PCL/CNS samples (PCL, PCL1f, PCL3f, PCL7f, and PCL1t) are reported in Table I.

In the case of SWCNTs we report the results of the 1% wt, to show the high outcome of the nanotube in the thermal properties and compare the effect of two different kinds of CNS at the same content values, as previously reported.[13]

The first heating scan is not reported since it is affected by solvent casting method and by all previous thermal history, it can not be representative of the CNS effect on polymer thermal properties.

In the cooling step, crystallization temperature (T_c) increased of around 10°C (Fig. 4) in PCL1f and PCL1t samples respect to neat PCL, that underlines the presence of a PCL crystal nucleation on CNS boundaries.[41] Carbon nanotubes induced a broader shift of T_c respect to CNFs with two overlapped peaks, since the PCL/SWCNT interaction enables the presence of the PCL/SWCNT interphase.[42] Similar behavior can be observed in the heating scans. PCL1t and PCL1f melting temperatures showed a 4°C increase compared to pure PCL (60°C) film, measured in the first heating scan. This shift confirmed that polymer organizes itself along the PCL/CNS interface with improved order and crystal length.[8] The interphase around SWCNT sidewalls is a micrometric polymer region with heterogeneous characteristics respect to bulk. The interphase properties depend on the aspect ratio of the nanostructure and they can affect the sample bulk response.[43] A broad distribution of crystal sizes in the region of the interphase is associated to SWCNT dispersion.

PCL/CNF hybrid materials showed a shift in the crystallization temperatures (T_c), which increases regularly with CNF percentage, from 10°C in PCL1f, until 14°C in PCL7f samples.[20] The nucleation effect of CNFs demonstrated by the calorimetry results is also an indication of the level of dispersion of the CNF in the PCL matrix. A slight increase of the crystallinity degree is measured by first melting scan (χ_{m1}) in PCL1f samples, while χ_{m1} decreased or remained unchanged in the other PCL/CNF samples, since the heterogeneous nucleation in PCL3f and PCL7f leads to the formation of more defects and less ordered PCL crystals.[20] The crystallinity degree measured in the cooling scan, χ_c, was reduced in all PCL/CNS specimens, in particular, from 50% (PCL) to 43% (PCL1t). SWCNTs enhance the crystal nucleation but reduce the polymer chain ability to be fully incorporated into growing crystals.[44] In the PCL/CNF samples, the heterogeneous nucleation leads to more defects around CNF sidewalls and to inhibition of the growing crystals during the cooling crystallization.[20]

A significant decrease of χ_{m2} respect to χ_{m1} can be observed in all PCL and composite samples. This

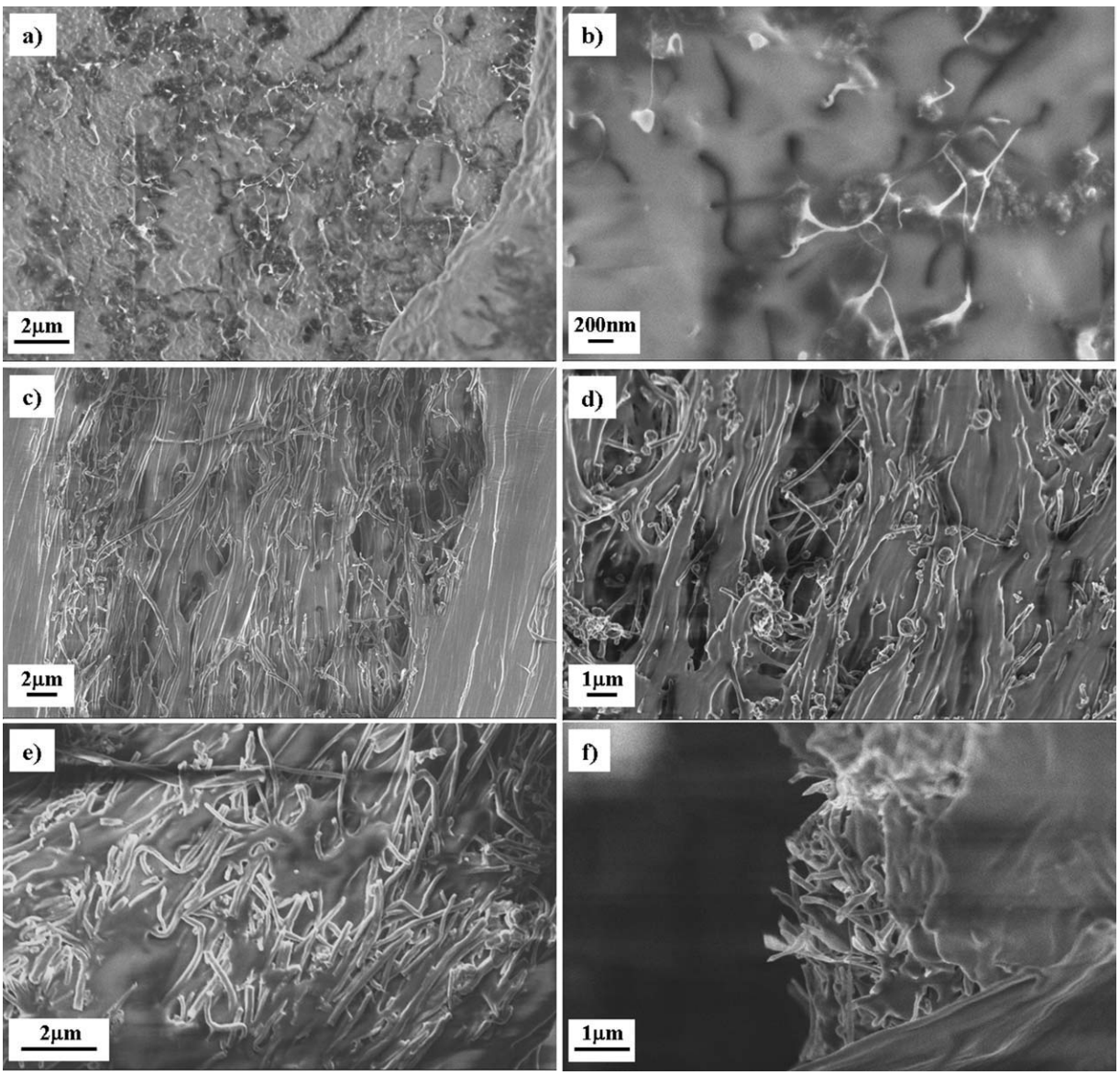

Figure 3 FESEM images of solvent cast PCL1t (a,b), PCL1f (c,d), and PCL3f (e,f) at low and high magnification.

result can be explained by the difference between the DSC dynamic crystallization against the slow solvent evaporation, which induced more *meta*-stable/amorphous polymer phase present in the scanned samples.[45]

An increase of χ_{m2} respect to χ_c can be detected only in composite samples, since CNS could affect the reorganization of crystals during heating; this effect is not revealed in PCL film.

Mechanical properties

Tensile properties of neat PCL and hybrid PCL/CNS samples were investigated and mechanical data are reported in Table II.

Tensile test of the composite samples based on CNFs (PCL, PCL1f, PCL3f, PCL7f) were investigated to analyze the role of the CNF content on the PCL mechanical properties. Moreover, to compare the results with another CNS at the same percentage, PCL1t was also investigated.

A stiffness enhancement was detected with increasing CNF content.[20] Reinforcing effects that rise up tensile modulus and inhibit drawing[46] of PCL/CNF specimens were observed. The effect of CNFs on drawing[47] was exhibited by PCL1f samples with a reduction of σ_b from 21 to 17 MPa and a reduction of ε_b from 1050 to 710%. Drawing inhibition is related to CNF dispersion in the PCL polymer, since the CNFs are able to hinder the chain sliding. Moreover PCL/CNF samples show a rigidity increase as a function of CNF content. In particular, the slight reduction of ε_y and σ_y indicates a material embrittlement and the increase of Young modulus confirms the rigidity enhancement in PCL1f samples.[48] Traditional reinforcing effects[49] are

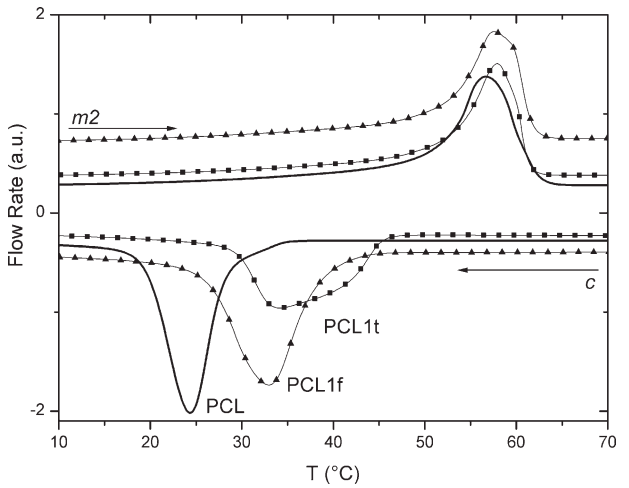

Figure 4 Cooling (*c*) and second heating (*m2*) scans corresponding to PCL, PCL1t, and PCL1f nanohybrid samples.

also detected in PCL7f and in PCL3f. The Young modulus is progressively raised up, and it reaches up one order of magnitude, increasing from 161 MPa of the neat PCL to 1400 MPa in the PCL7f.

PCL/SWCNT tensile properties are also investigated and reported in Table II, and they show different mechanical behavior from CNF composites. An interesting stiffness-yielding coexistence is observed that indicates a toughness improvement. In these composites, σ_b increases without reducing ε_b.

SWCNTs can render the material more stiff, since the increase of σ_b proceeds with an increase of the Young modulus that reaches 220 MPa. In front of these hardening effects, the elongation at break and the yield strain are not compromised by SWCNTs, ε_b and ε_y are improved by a toughness effect till 1360 and 18%, respectively.

TABLE I
Data Related to DSC Thermograms of Neat PCL and Nanohybrid PCL/CNS Samples

Samples	T_{m1} (°C)	T_c (°C)	T_{m2} (°C)
PCL	60.4 ± 0.5	24.5 ± 0.1	56.5 ± 0.4
PCL1f	64 ± 1	34 ± 1	57.0 ± 0.4
PCL3f	62.7 ± 0.5	35.3 ± 0.1	57.6 ± 0.1
PCL7f	62.8 ± 0.3	38.4 ± 0.1	57.1 ± 0.1
PCL1t	64.4 ± 0.7	33.9 ± 0.1	58.1 ± 0.2
	ΔH_{m1} (J/g)	ΔH_c (J/g)	ΔH_{m2} (J/g)
PCL	85.8 ± 0.6	68.4 ± 0.2	68.2 ± 0.1
PCL1f	87 ± 1	59.2 ± 0.9	66.3 ± 0.8
PCL3f	83 ± 1	59.1 ± 0.1	67 ± 1
PCL7f	77.1 ± 1.6	56.2 ± 0.7	65 ± 1
PCL1t	73.8 ± 2.1	57.9 ± 1.4	63.8 ± 1.4
	χ_{m1} (%)[a]	χ_c (%)[b]	χ_{m2} (%)[c]
PCL	63.0 ± 0.1	50.3 ± 0.2	50.2 ± 0.1
PCL1f	64.6 ± 0.7	44.4 ± 0.6	49.2 ± 0.6
PCL3f	62.8 ± 0.1	44.3 ± 0.1	50.3 ± 0.2
PCL7f	61.2 ± 0.8	44.0 ± 0.5	51.5 ± 1.1
PCL1t	54.8 ± 1.7	43.1 ± 0.6	47 ± 1

Crystallinity degree (%) referred to first melting (a); second melting (b); cooling scan (c).

TABLE II
Mechanical Properties of Hybrid PCL/CNS Materials in Failure Tensile Test

Samples	σ_b (MPa)	ε_b (%)	σ_y (MPa)	ε_y (%)	E (MPa)
PCL	21 ± 1	1050 ± 20	10.9 ± 0.5	16.7 ± 0.9	161 ± 9
PCL1f	17.7 ± 0.7	710 ± 30	9.9 ± 0.9	10 ± 1	310 ± 40
PCL3f	23.9 ± 1.1	760 ± 50	16.7 ± 0.9	16 ± 1	420 ± 20
PCL7f	25 ± 1	360 ± 70	23.4 ± 1.7	6 ± 1	1450 ± 90
PCL1t	23.1 ± 0.6	1360 ± 40	12.3 ± 0.9	18 ± 1	220 ± 20

DMA analysis was performed on PCL/CNS hybrid samples to verify the effect of CNS type and percentage on polymer shear properties.[50] The strength of the PCL/CNS interaction may result from molecular-level entanglement and forced long-range ordering of the polymer.[21] Figure 5(a) shows storage modulus of PCL, PCL0.5f, PCL1f, and PCL7f composites.

DMA measurements were performed also at low CNF concentration (0.5 wt %), since the analysis is sensitive to interface response that is improved by high polymer/CNF surface interaction.

The PCL shear modulus is improved in PCL1f but not in PCL7f samples showing the embrittlement effect mentioned in tensile results. CNFs are able to generate entanglements with PCL but above 1% wt, they act as local stress raisers and PCL around CNF sidewalls absorb preferentially the amplified shear load. The high CNF amount can induce a ductile to brittle transition at low frequency test.

Figure 5(b) shows the dynamo-mechanical properties of PCL/SWCNTs samples. Shear modulus increased in the nanohybrid samples based on SWCNTs, as a function of carbon nanotube content (PCL, PCL0.5t, PCL0.75t, PCL1t). The SWCNT aspect ratio has a positive effect in the physical interaction and entanglement with polymer chains. Good interfacial adhesion between fillers and polymer matrix is essential for efficient load transfer in the composite.[51] The entanglement level and the physical interaction between CNS and biopolymer is the main factor in the mechanical response when a chemical adhesion is not assured.[52]

Traditional mechanical response characterized the PCL/CNF samples as confirmed by brittleness of PCL7f films in DMA test while an innovative behavior was revealed by PCL/SWCNT composites that increased tenacity.[53] This result can be associated with the wide continuous distribution of PCL crystals in the PCL/SWCNT interphase that permits a more efficient load transfer and absorption respect to CNF-based samples.

Dielectric properties

Figure 6 summarizes dielectric measurements of PCL and PCL/CNS composites.

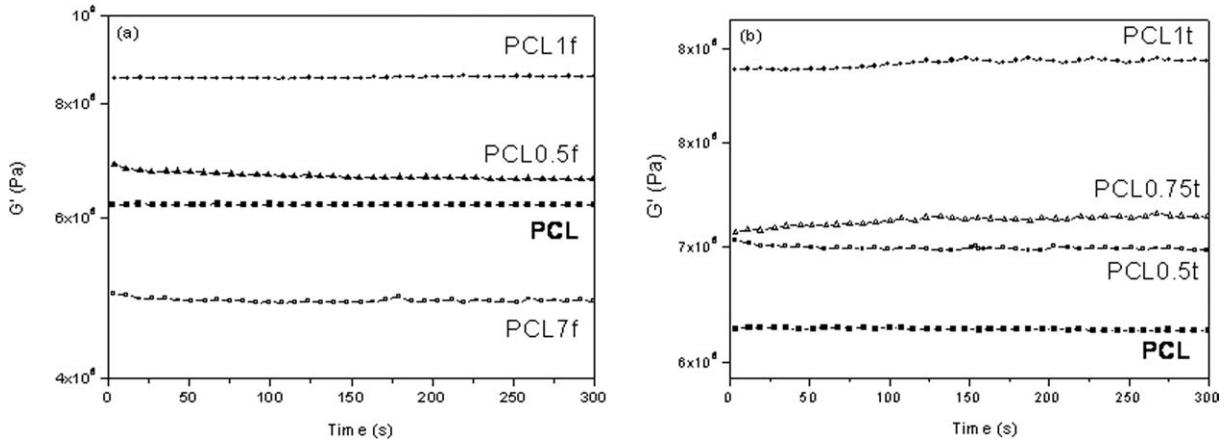

Figure 5 DMA dynamic time sweep test on hybrid PCL/CNS samples for different percentage of CNFs (a) and SWCNTs (b).

To study the dielectrical behavior and evaluate the electrical percolation threshold,[54] composite films based on SWCNTs at 0.5, 0.75, or 1% wt respect to PCL weight (PCL0.5t, PCL0.75t, PCL1t) were investigated.[34]

Figure 6(a,b) show the frequency dependence (log–log plot) of the bulk AC conductivity of PCL/CNF and PCL/SWCNT samples, respectively. The PCL polymer is an ideal dielectric material and displays an increase in the capacitive component with increasing frequency. The bulk AC conductivity of the neat PCL film increases linearly (from 10^{-9} to 10^{-4} S/cm) as the frequency increases from 20 Hz to 1 MHz.

Composites with CNF content lower than 3% wt show a purely insulating behavior, as indicated by the frequency-dependent increase in conductivity on the log–log plot of specific conductivity against

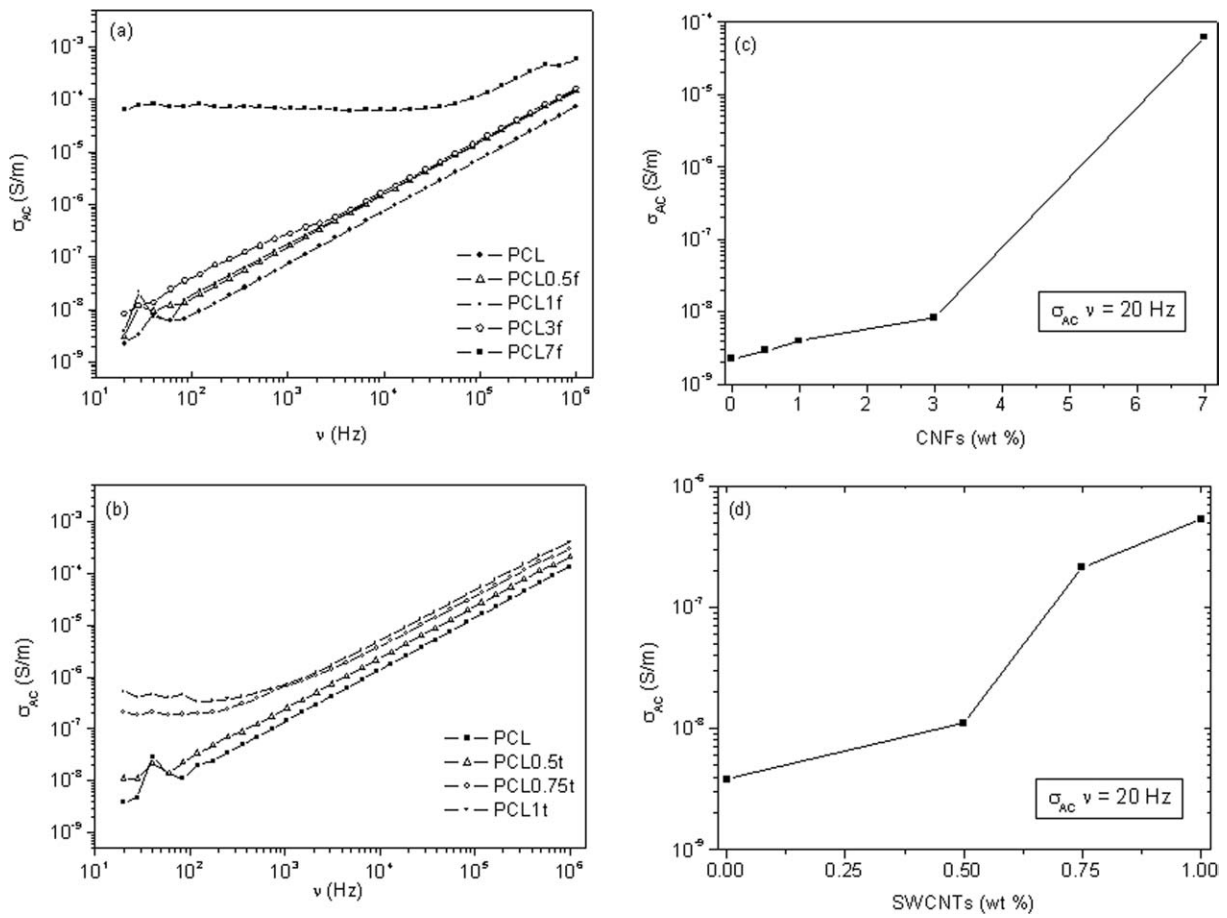

Figure 6 The frequency-dependent (log–log plot) of the bulk AC conductivity of PCL/CNF composites (a), on PCL/SWCNTs (b), and AC conductibility at 20 Hz corresponding to different CNFs (c) or SWCNTs (d) percentages.

frequency.[55] A different behavior is obtained increasing CNF content, in fact in PCL7f samples conductivity remain constant at a given frequency range.[56] Figure 6(c) shows the conductivity of PCL/CNF composites at different CNF content and frequency of 20 Hz. The results show that conductivity increases by four order of magnitude, as the nanofiber content reaches 3 wt. %

Figure 6(b,d) shows dielectric measurements of PCL/SWCNT composites. Few SWCNT percentage (0.75% wt) enhances the electrical conductivity of PCL polymer. The linear trend of σ_{ac} with the frequency is evident below 0.5% wt SWCNT content. A different behavior was obtained in the PCL0.75t and PCL1t samples that show a conductive manner. The conductivity of PCL/SWCNT samples significantly increased above 0.75% wt SWCNTs [Fig. 6(d)].

Dielectric measurements highlight the importance of CNS clustering for the formation of a conductive network. The change in AC conductivity with frequency provides information about the overall connectivity of the CNS conducting network.

CONCLUSIONS

PCL composite films with CNS were produced by solvent casting and characterized. The combination of results in terms of morphological, mechanical, thermal, and electrical analysis represented the main novelty of this article, to elucidate the effects of different CNS on PCL properties.

A modulation of the properties in the range of CNS analyzed concentrations represented an important issue of the article.

Novel and enhanced properties of PCL/CNS composites revealed the strong effects of the CNS on the polymer behavior with particular focus on the mechanical reinforcing effects and the electrical conductivity.

CNFs affected the crystallization of PCL polymer, increased the PCL stiffness and electrical conductivity. It is interesting to note that no functionalization on CNFs was required to obtain good electrical conductivity combined with mechanical reinforcement on PCL/CNF composites.

SWCNTs improve the PCL electrical conductivity at very low concentrations and the interaction with the polymer matrix enables the presence of the PCL/SWCNT interphase, as revealed by the shoulder in the cooling DSC thermogram.

These studies suggest that the combination of polymer matrix with different CNS offers a strategic way for the self-assembly of nanomaterials and nanodevices with tunable thermal, mechanical, and electrical properties. These novel electrical current-conducting materials, as CNS polymer composites, offer very promising opportunities for the development of new polymer-based electrical devices. Improving the solvent casting method will be the next important step toward controlled and individual distributions of CNS in the polymer matrix.

The author, D.M., gratefully acknowledges the Biostructures and Biosystems Italian Institute, I.N.B.B. for financial support. The author I.A. is supported by National INSTM Consortium.

References

1. Honma, I.; Nakajima, H.; Nomura, S. Solid State Ionics 2002, 154, 707.
2. Njuguna, J.; Pielichowski, K.; Desai, S. Polym Adv Technol 2008, 19, 947.
3. Zavyalo, S. A.; Pivkina, A. N.; Schoonman, J. Solid State Ionics 2002, 147, 415.
4. Chiang, C. K.; Popielarz, R.; Sung, L. P. Mat Res Soc Symp Proc 2001, 682E, 691.
5. Jäger, K. M.; McQueen, D. H.; Tchmutin, I. A.; Ryvkina, N. G.; Kluppel, M. J Phys D: Appl Phys 2001, 34, 2699.
6. Vlasvelda, D. P. N.; De Jong, M.; Bersee, H. E. N.; Gotsis, A. D.; Picken, S. Polymer J 2005, 46, 10279.
7. Jordana, J.; Jacob, K. I.; Tannenbaum, R.; Sharaf, M. A.; Jasiuk, I. Mater Sci Eng A Struct Mater: Prop Microstruct Process 2005, 393, 1.
8. Chen, E. C.; Wu, T. M. Polym Degrad Stab 2007, 92, 1009.
9. Lepoittevin, B.; Devalkenaere, M.; Pantoustier, N.; Alexandre, M.; Kubies, D.; Galberg, C. Polym J 2002, 43, 4017.
10. Li, G.; Gill, T. J.; De Frate, L. E.; Zayontz, S.; Glatt, V.; Zarins, B. J Orthop Res 2002, 20, 887.
11. Chew, S. Y.; Hufnagel, T. C.; Lim, C. T.; Leong, K. W. Nanotechnology 2006, 17, 3880.
12. Kymakis, E.; Alexandou, I.; Amaratunga, G. A. Synth Met 2002, 127, 59.
13. Valentini, L.; Puglia, D.; Frulloni, E.; Armentano, I.; Kenny, J. M.; Santucci, S. Compos Sci Technol 2004, 64, 23.
14. Ma, C.; Zhang, W.; Zhua, Y.; Ji, L.; Zhanga, R.; Koratkar, N. Carbon 2008, 46, 706.
15. Zhang, Q.; Rastogi, S.; Chen, D.; Lippits, D.; Lemstra, P. J. Carbon 2006, 44, 778.
16. Hammel, E.; Tang, X.; Trampert, M.; Schmitt, T.; Mauthner, K.; Eder, A. Carbon 2004, 42, 1153.
17. Sui, G.; Jana, S.; Zhong, W. H.; Fuqua, M. A.; Ulven, C. A. Acta Mater 2008, 56, 2381.
18. Hu, Y.; Shenderova, O. A.; Hu, Z.; Padgett, C. W.; Brenner, D. W. Rep Prog Phys 2006, 69, 1847.
19. Treacy, M. M. J.; Ebbesen, T. W.; Gibson, T. M. Nature 1996, 381, 680.
20. Armentano, I.; Del Gaudio, C.; Bianco, A.; Dottori, M.; Nanni, F.; Fortunati, E.; Kenny, J. M. J Mater Sci 2009, 44, 4789.
21. Thostenson, E. T.; Ren, Z.; Chou, T. W. Compos Sci Technol 2001, 61, 1899.
22. Yogeeswaran, G.; Jun, L. JOM 2009, 61, 32.
23. Xie, S.; Li, W.; Pan, Z.; Chang, B.; Sun, L. J. Phys Chem Solids 2000, 61, 1153.
24. Brandl, W.; Marginean, G.; Chiril, V.; Warschewski, W. Carbon 2004, 42, 5.
25. Song, H.; Zhang, Z.; Men. X. H. Eur Polym J Macromol Nanotechnol 2007, 43, 4092.
26. Tjong, S. Mater Sci Eng R 2006, 53, 73.
27. Wagner, H. D.; Vaia, R. A.; Mater Today 2004, 7, 38.
28. Coleman, J. N.; Curran, S.; Dalton, A. B.; Davey, A. P.; McCarthy, B.; Blau, W. Phys Rev B: Condens Matter 1998, 58, 7492.

29. Mitchell, C. A.; Krishnamoorti, R. Macromolecules 2007, 40, 1538.
30. Chatterjee, T.; Mitchell, C. A.; Hadjiev, V. G.; Krishnamoorti, R. Adv Mater 2007, 19, 3850.
31. Tsubokava, N. Polymer J 2005, 37, 637.
32. Se-Jin, O.; Hwa-Jeong, L.; Dong-Ki, K.; Seong-Woo, L.; David, H. W.; Soo-Young, P. Polymer J 2006, 47, 1132.
33. Tang, Z. G.; Black R. A.; Curran, J. M.; Hunt, J. A.; Rhodes, N. P.; Williams, D. F. Biomaterials 2004, 25, 4741.
34. Wang, L. Z.; Dang, M. Appl Phys Lett 2005, 87, 429.
35. Higgins, B. A.; Brittain, W. J. Eur Polym J 2005, 41, 889.
36. Guo, Q.; Harrats, C.; Groeninckx, G.; Reynaers, H.; Koch, M. H. J. Polymer J 2001, 42, 6031.
37. Mathur, R. B.; Seth, S.; Lal, C.; Singh, B. P.; Dhami, T. L.; Rao, A. M. Carbon 2007, 45, 132.
38. Mansfield, E.; Kar, A.; Hooker, S. A. Anal Bioanal Chem 2010, 396, 1071.
39. Armentano, I.; Dottori, M.; Puglia, D.; Kenny, J. M. J Mater Sci: Mat Med 2008, 19, 2377.
40. Lacerda, L.; Bianco, A.; Prato, M.; Kostarelos, K. Adv Drug Deliv Rev 2006, 58, 1460.
41. Jiang, S.; Ji, X.; An, L.; Jiang, B. Polymer 2001, 42, 3901.
42. Ryan, K. P.; Cadek, M.; Walker, V.; Ruether, S.; Fonseca, M. Synth Met 2006, 156, 332.
43. Masud, A. K. M.; Tahreen, N.; Abedin, F. J Mech Eng 2009, 40, 29.
44. Wu, D.; Wu, L.; Sun, Y.; Zhang, M. J Polym Sci B: Polym Phys 2007, 25, 3137.
45. Saunders, M.; Podluii, K.; Shergill, S.; Buckton, G.; Royal, P. Int J Pharm 2004, 274, 35.
46. Roylance, D. Mechanics of Materials, Ed.; John Wiley & Sons: New York, 1996.
47. Leonov, A. I. Int J Solid Struct 2002, 39, 5913.
48. Frankland, S. J. V.; Harik, V. M.; Odegard, G. M.; Brenner, D. W.; Gates, T. S. Compos Sci Technol 2003, 63, 1655.
49. Vaia, R. A.; Wagner, H. D. Mater Today 2004, 7, 32.
50. Frankland, S. J. V.; Caglar, A.; Brenner, D. W.; Griebel, M. J Phys Chem B 2002, 106, 3046.
51. Andrews, R.; Weisenberger, M. C. Curr Opin Solid State Mater Sci 2004, 8, 31.
52. Odegard, G. M. Nanoengineering of Structural, Functional and Smart Materials; CRC Press LLC: USA, 2005; Vol. C23, p 621.
53. Odegard, G. M.; Gates, T. S.; Wise, K. E.; Park, C.; Siochi, E. J. Compos Sci Technol 2003, 63, 1671.
54. Jimenez, G. A.; Jana, S. C. Compos Part A Appl Sci Manuf 2007, 38, 983.
55. Martin, C. A.; Sandler, J. K. W.; Shaffer, M. S.; Schwarz, M. K.; Bauhofer, W.; Schulte, K. Compos Sci Technol 2004, 64, 2309.
56. Kim, Y. J.; Shin, H. D.; Choi, T. S.; Kwon, J. H.; Chung, Y. C.; Yoon, H. G. Carbon 2005, 43, 23.